EFFECT OF COIL SURFACE AREA ON THE HEMODYNAMICS OF A PATIENT-SPECIFIC INTRACRANIAL ANEURYSM: A COMPUTATIONAL STUDY

M. L. Aguilar[⋆†], *H. G. Morales*[⋆†], *I. Larrabide*[†⋆], *J. M. Macho*[‡], *L. San Roman*[†], *and A. F. Frangi*[⋆†§]

[⋆] Center for Computational Imaging & Simulation Technologies in Biomedicine (CISTIB) – Universitat Pompeu Fabra (UPF), Barcelona, Spain
[†] Networking Center on Biomedical Research (CIBER-BBN), Barcelona, Spain
[‡] Department of Radiology, Hospital Clínic, Barcelona, Spain
[§] Department of Mechanical Engineering, University of Sheffield, Sheffield, UK.

ABSTRACT

The purpose of this work is to evaluate the influence of coil diameters on the hemodynamics of intracranial aneurysms by using computational fluid dynamic (CFD) simulations. Three virtual treatments were performed varying packing density and coil surface area, by changing coil diameter. Hemodynamic parameters such as wall shear stress (WSS), average velocity and dye concentration at the aneurysm site were qualitative and quantitatively analyzed. Simulations with same coil area (958 mm^2) but different packing density (21.0% and 41.6%) show similar hemodynamic alterations. Besides, the treated model with the highest coil area (1596 mm^2) and intermediate packing density (33.2%) exhibited the highest reduction in the studied hemodynamic variables. Our findings show that coil area plays an important role in the resistance (pressure and frictional drags) of blood flow through the coils.

Index Terms— intracranial aneurysms, endovascular coiling, CFD, coil surface area, hemodynamics

1. INTRODUCTION

Endovascular treatment of intracranial aneurysms using coil embolization techniques has been a common practice in the last decades [1]. This treatment involves guiding a microcatheter to the aneurysm site to insert biocompatible wires of microscopic dimensions, better known as coils. They are meant to promote a hemodynamic environment suitable for thrombosis inside the aneurysm cavity, which would subsequently lead to parent vessel patency and lessen rupture risk. Clinicians attempt to insert as many coils as possible since packing density (the ratio between the inserted coil volume and aneurysm volume) has been related to reduced aneurysm recanalization [2, 3]. However, the risk of aneurysm perforation, coil migration or mass effect constrains greatly the final packing density. It has been reported that a mean of 23% and a maximum of 40% can be achieved with standard Guglielmi detachable coils [3].

There are several types of coils available in the market [4] and most of their features are meant to improve both operative performance (coil flexibility) and packing density. However, the influence on intra-aneurysmal hemodynamics due to the presence of different coil types, in particular different coil diameters, has not been considered yet. Pressure and friction drags exerted by blood flow onto the coil depend on the contact surface; and therefore, similar drags may occur if the same area is used at different packing densities, which can be achieved by varying the coil diameter. The purpose of this work is to evaluate the influence of coil diameters, packing density, and coil surface area on intra-aneurysmal hemodynamics by using CFD simulations.

2. MATERIALS

A saccular aneurysm, located on the ophthalmic segment of the left internal carotid artery, of a 42-year-old woman was studied in this work. A three-dimensional rotational angiography (3DRA) image of the aneurysm was captured with an AXIOM Artis (Siemens Medical Solutions, Erlangen, Germany). The 3DRA field of view used was 194.75 mm with a reconstruction matrix of 512x512x442 (Figure 1(a)). The dimensions of the aneurysm were 6.6 mm for neck diameter, 7.5 mm for dome depth and a volume of 280 mm^3. According to patient condition and current clinical practice, the aneurysm was suitable for endovascular coil treatment.

The research leading to these results has received funding from the European Union Seventh Framework Programme (FP7/2007-2013) under grant agreement nr 223920, VPH-NoE project, has been partially funded by the Industrial and Technological Development Center (CDTI) under the CENIT-cvREMOD program and the Catalonian Department of Innovation, Universities and Enterprise (DIUE), through the EndoTreat project (exp. VALOR2010-00064). Alejandro F. Frangi is partially funded by the ICREA-Academia programme.

Model	*M0*	*M1*	*M2*	*M3*
Coil diameter [mm]	–	0.508	0.254	0.254
Length [mm]	–	575	1165	1835
Area [mm^2]	–	958	958	1596
Packing density [%]	0.0	41.6	21.0	33.2

Table 1: Description of the models used in this study.

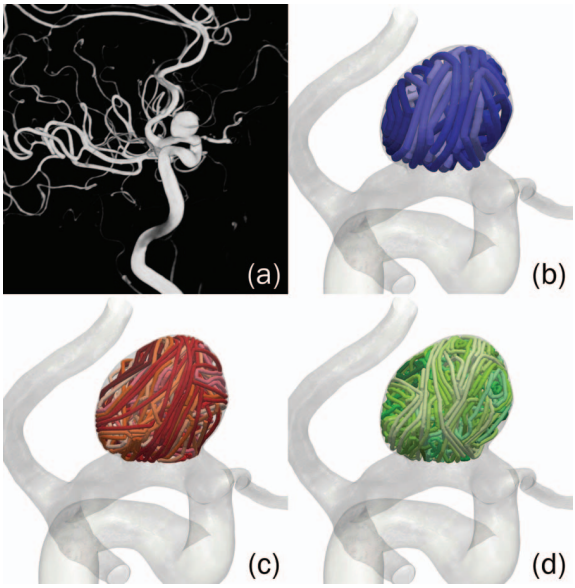


Fig. 1: (a) Volume rendering of the vessel. (b - d) Vascular models of treatments 1, 2, and 3, respectively.

3. METHODS

3.1. Image Processing

The medical images were used to reconstruct the vascular region of interest, which includes the aneurysm, the internal carotid artery, and the vessels immediately distal to the aneurysm. From this region of interest, a surface mesh was extracted using a segmentation algorithm based on geodesic active regions [5]. The surface mesh was cleaned and smoothed using in-house software, GIMIAS [6].

3.2. Virtual Coiling

The aneurysm geometry was virtually treated with endovascular coils. An untreated (M0) and three coiling models were considered in this study (see Table 1). The first coiling model (M1) considered a high packing density of 41.6% using six 0.508 mm-diameter coils. The second model (M2) has the same coil area as M1, but uses thinner coils of 0.254 mm of diameter. These thinner coils provide a packing density of only 21.0%. Finally, the third coiled model (M3) uses the same coil diameter as M2, but with a packing density between the ones of M1 and M2 (33.2%).

To create the coils, a technique based on a dynamic path planning was used [7]. Basically, the technique deploys the coils one-by-one until the desirable packing density is achieved. Aneurysm perforation, coil collision and migration are not allowed. Additionally, the technique is able to retract and redirect the tip of the coil being inserted when it is blocked by previously inserted coils. To preserve the coils inside the aneurysm, a surface is added at the aneurysm ostium making it a closed surface. Figure 1(b-d) shows the final configuration of the coils for each coiling model.

3.3. Meshing and CFD

Volumetric meshes, composed of unstructured tetrahedral and 8-node prism elements, were generated for each of the models using ANSYS ICEM CFD v12 (Ansys Inc., Canonsburg, PA, USA) commercial software. Maximum global element size was 0.3 mm, where elements of the mesh would gradually refine themselves towards the wall into a size of 0.15 mm. The element size around the coils was 0.06 mm. The total number of volumetric elements generated for models M0 through M3 were 0.74 million, 6.75 million, 7.59 million, 10.96 million, respectively.

Using ANSYS CFX v12, continuity and momentum equations were solved throughout the volumetric mesh. The vessel wall and coils were set to be rigid with no-slip boundary condition. Blood was considered as an incompressible Newtonian fluid with a viscosity of 0.0035 Pa·s and density of 1066 kg/m^3. Flow boundary conditions were imposed according to a one-dimensional mathematical model of the systemic tree, which was developed within the @neurIST project [8]. A mass flow rate was imposed at the inlet, whereas pressure was imposed at the outlets. Three cardiac cycles of 0.8 s each were computed, but the first one was considered only to achieve numerical stability. Each cardiac cycle period was divided into time steps of 0.005 s.

To simulate an injection and transport of a contrast dye, a massless scalar field was solved using a transport equation obtained from literature [9]. The propagation of the contrast dye started at the beginning of the second cardiac cycle at a constant rate of one, and continued until the beginning of the third cycle which allowed visualization of the washout phase.

Data from the last two cardiac cycles was stored to analyze intra-aneurysmal hemodynamic alterations after coiling. The hemodynamic activity was evaluated from WSS, average velocity and dye concentration inside the aneurysm. These variables were considered since changes in hemodynamics have been correlated with physiological response [10, 11].

Quantitatively, variations throughout the third cardiac cycle were obtained for WSS and velocity inside the aneurysm dome. Dye concentration was evaluated from the start of the injection to the end of the third cycle. Qualitatively, WSS and

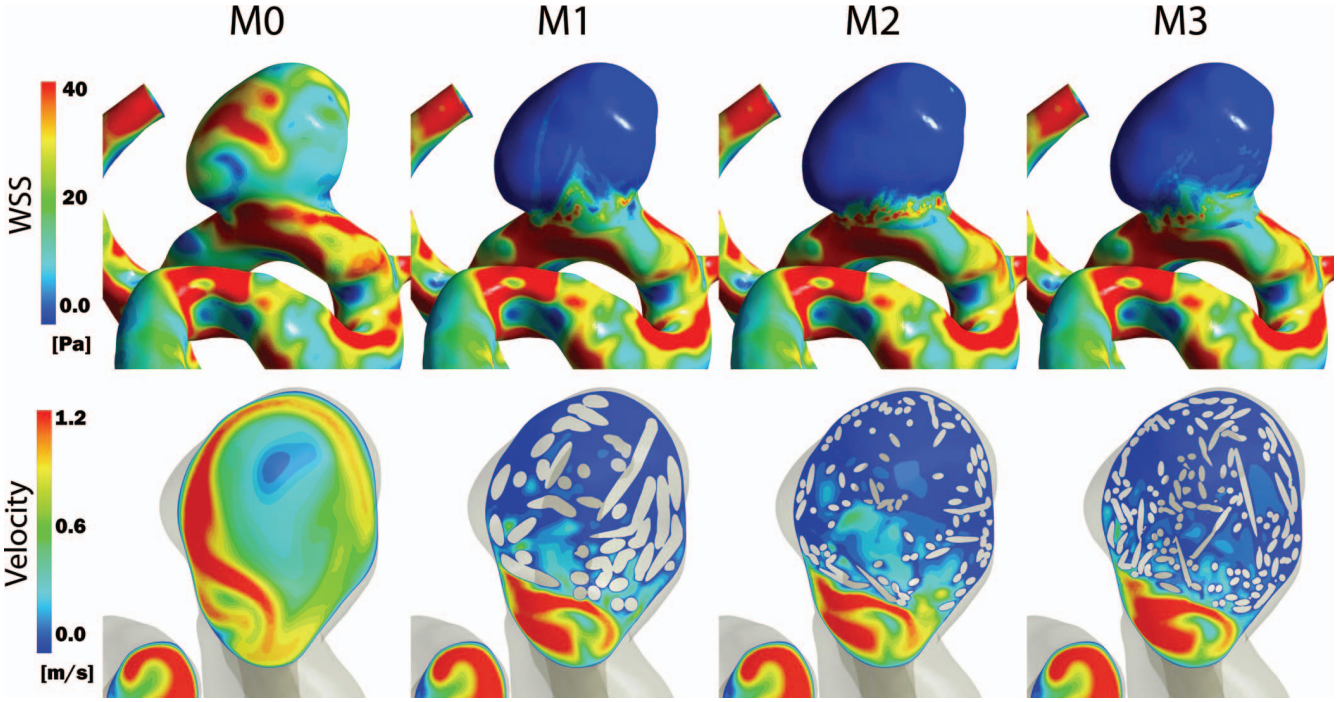


Fig. 2: WSS distribution and velocity contours in a cut plane, at peak systole for all models.

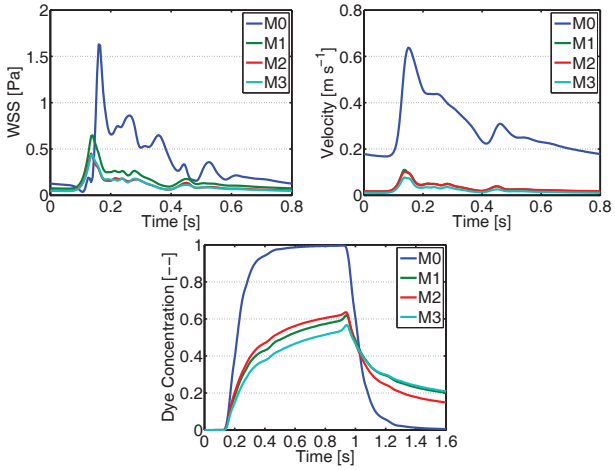


Fig. 3: Variations of intra-aneurysmal hemodynamic parameters throughout time.

velocity were observed at peak systole.

4. RESULTS

4.1. Qualitative results

Figure 2 shows contour plots for WSS and velocity on the four models. M0 presents high WSS (>40 Pa) at the distal side of the aneurysm wall, which is associated to the impingement of the blood flow jet at that zone. Flow inside the aneurysm is characterized by a singular vortical structure.

In the treated models, it is visualized that both variables, WSS and flow velocity, were decreased after coiling. Also, they show similar flow alterations compared to M0, although local singularities in the WSS distributions (especially at the aneurysm neck) and velocities inside the aneurysm appear due to the particular coil distribution of each treated model.

4.2. Quantitative results

Figure 3 shows the variations of WSS and velocity along one cardiac cycle and dye concentration during filling and washout phases. Compared to M0, all parameters have been reduced after coiling.

Time-averaged reductions in WSS induced by coiling were 55.5%, 69.5%, and 70.5% for M1, M2, and M3, respectively. Regarding time-averaged velocity inside the aneurysm volume, both M1 and M2 have similar velocity reduction of 88.8%. M3 has reduced velocity by 92.3%.

Dye concentration curves show that all treated models have a similar dye concentration evolution in time. In general, the amount of dye entering the aneurysm was reduced and its stay was prolonged.

5. DISCUSSION

In this work, CFD simulations were performed on a patient-specific cerebral aneurysm model. The purpose was to in-

vestigate the influence on intra-aneurysmal hemodynamic alterations due to different coil diameters. We found that qualitative differences among the treated models are negligible and similar tendencies appear when hemodynamic parameters are observed throughout time. In general, all treated models present reduction of the intra-aneurysmal velocity and WSS, as well as decrease of the dye concentration entering the aneurysm and increase of its residence time. These hemodynamic alterations after coiling have been visualized in experiments with phantoms [12, 13, 14].

For M1 and M2, both having the same coil area of contact with flow but different packing density (M2 has half the packing density of M1), similar hemodynamic alterations were found. These results confirm that coil area plays an important role in the resistance (pressure and frictional drags) of blood flow through the coils. Furthermore, M3, presenting the highest surface area of coils among all models and a packing density (33.2%) lower than the one of M1 (41.6%), exhibited a higher reduction for velocity and dye concentration. This finding shows that the coil area is an important parameter to have in consideration when treating an intracranial aneurysm with endovascular coiling.

Although all parameters have been greatly reduced for the treated models, we can not establish if these hemodynamic conditions are the ones that trigger the coagulation cascade. The use of CFD studies in correlation with clinical events (e.g., aneurysm occlusion/recanalization in follow-up) is one way to overcome these issues.

6. CONCLUSIONS

Using CFD along with the virtual coiling algorithm provides a mean to study the hemodynamic alterations induced by different treatment options. It is observable that all treatment options reduced the intra-aneurysmal velocity, WSS, and dye concentration in comparison to the untreated computational model. For this aneurysm in particular, changes in hemodynamic condition depend on packing density as much as on coil surface area in contact with blood flow. A high coil surface area increases pressure and frictional drags, leading to flow stasis (low velocity and high dye residence time). Thereby, it should be taken into account for endovascular coil treatment. Further studies performed on a larger dataset of patient aneurysm models are required to better understand the implications of using different coil diameters.

7. REFERENCES

[1] G. Guglielmi, "History of the genesis of detachable coils," *Journal of Neurosurgery*, vol. 111, no. 1, pp. 1–8, 2009.

[2] Y. Kawanabe, A. Sadato, W. Taki, and N. Hashimoto, "Endovascular occlusion of intracranial aneurysms with guglielmi detachable coils: correlation between coil packing density and coil compaction," *Acta Neurochir (Wien)*, vol. 143, no. 5, pp. 451–455, 2001.

[3] M. Sluzewski, W.J. van Rooij, M.J. Slob, J.O. Bescós, C.H. Slump, and D. Wijnalda, "Relation between aneurysm volume, packing, and compaction in 145 cerebral aneurysms treated with coils," *Radiology*, vol. 231, no. 3, pp. 653–658, 2004.

[4] J.B. White, C.G.M. Ken, H.J. Cloft, and D.F. Kallmes, "Coils in a nutshell: A review of coil physical properties," *American Journal of Neuroradiology*, vol. 29, no. 7, pp. 1242–1246, 2008.

[5] H. Bogunović, J.M. Pozo, M.C. Villa-Uriol, C.B.L.M. Majoie, R. van-den Berg, H.A.F.G. van Andel, J.M. Macho, J. Blasco, L. San Roman, and A.F. Frangi, "Automated segmentation of cerebral vasculature with aneurysms in 3DRA and TOF-MRA using geodesic active regions: An evaluation study," *American Journal of Neuroradiology*, vol. 38, no. 1, pp. 210–222, 2011.

[6] I. Larrabide, P. Omedas, Y. Martelli, X. Planes, M. Nieber, J. Moya, C. Butakoff, R. Sebastián, O. Camara, M. De Craene, B. Bijnens, and A.F. Frangi, "GIMIAS: An open source framework for efficient development of research tools and clinical prototypes," in *Functional Imaging and Modeling of the Heart*, 2009, vol. 5528, pp. 417–426, www.gimias.org.

[7] H.G. Morales, I. Larrabide, M. Kim, M.C. Villa-Uriol, J.M. Macho, J. Blasco, L. San Roman, and A.F. Frangi, "Virtual coiling of intracranial aneurysms based on dynamic path planning," in *Medical Image Computing and Computer Assited Intervention (MICCAI). Toronto, Canada*, 2011, pp. 355–362.

[8] P. Reymond, F. Merenda, F. Perren, D.A. Rüfenacht, and N. Stergiopulos, "Validation of a one-dimensional model of the systemic arterial tree," *American Journal of Physiology. Heart and Circulatory Physiology*, vol. 297, no. 1, pp. H208–22, 2009.

[9] Q. Sun, A. Groth, M. Bertram, I. Waechter, T. Bruijns, R. Hermans, and T. Aach, "Phantom-based experimental validation of computational fluid dynamics simulations on cerebral aneurysms," *Medical Physics*, vol. 37, no. 9, pp. 5054–5065, 2010.

[10] A.M. Malek, S.L. Alper, and S. Izumo, "Hemodynamic shear stress and its role in atherosclerosis," *Journal of the American Medical Association*, vol. 282, no. 21, pp. 2035–2042, 1999.

[11] D.M. Wootton and D.N. Ku, "Fluid mechanics of vascular systems, diseases, and thrombosis," *Annual Review of Biomedical Engineering*, vol. 1, no. 1, pp. 299–329, 1999.

[12] S.G. Imbesi and C.W. Kerber, "Analysis of slipstream flow in a wide-necked basilar artery aneurysm: evaluation of potential treatment regimens," *American Journal of Neuroradiology*, vol. 22, no. 4, pp. 721–4, 2001.

[13] S. Rudin, Z. Wang, I. Kyprianou, K.R. Hoffmann, Y. Wu, H. Meng, L.R. Guterman, B. Nemes, D.R. Bednarek, J .Dmochowski, and L.N. Hopkins, "Measurement of flow modification in phantom aneurysm model: comparison of coils and a longitudinally and axially asymmetric stent–initial findings," *Radiology*, vol. 231, no. 1, pp. 272–6, 2004.

[14] M.H. Babiker, L.F. Gonzalez, F. Albuquerque, D. Collins, A. Elvikis, and D.H. Frakes, "Quantitative effects of coil packing density on cerebral aneurysm fluid dynamics: an in vitro steady flow study," *Annals of Biomedical Engineering*, vol. 38, no. 7, pp. 2293–301, 2010.